MORPHOLOGICAL QUANTIFICATION OF POLYMER NANOFIBERS IN TISSUE ENGINEERING IMAGES

M.A. GONZALEZ[†§], F. MONTINI BALLARIN[‡§], M. BRUN[†], G. ABRAHAM[‡] and V.L. BALLARIN[†]

† *Lab. Process and Measurement Signal Processing, School of Engineering UNMdP mazulgonzalez@fi.edu.ar*
‡ *Biomedical Polymers Group, INTEMA (UNMdP-CONICET) Mar del Plata.*
§ CONICET.

***Abstract*— The design and fabrication of highly porous polymeric or composite scaffolds for tissue engineering and organ regeneration are keystones to advance in these interdisciplinary research areas. The development of biocompatible polymeric matrices with particular morphologies that promote a specific biological response for each type of cell, is strongly needed. To attain this goal, the characterization and quantification of the morphological properties of the scaffolds are necessary to correlate them to mechanical and biological properties.**

In this work, micro/nanofibrous scaffolds obtained by electrospinning were characterized by scanning electron microscopy (SEM). The use of the granulometric size function, computed from the scaffold images, to develop algorithms that help the specialists in the characterization of the shape, size, stocking density and orientation of the arrays, is proposed. The obtained results show that the analysis of SEM images allows for a good characterization of fibrous scaffolds becoming a useful tool for specialists in this research area.

***Keywords*— Digital Image Processing, Mathematical Morphology, Tissue Engineering, Biomedical Polymers.**

I. INTRODUCTION

Tissue engineering is currently one of the most attractive areas of multi-and interdisciplinary research. Among other essential components, tissue engineering requires appropriate artificial extracellular matrices (ECM) in the form of highly porous scaffolds, able to regulate and stimulate the cellular functions of adhesion, migration, growth, differentiation and tissue organization (Ikada, 2006; Abraham *et al.*, 2007). The factors governing the properties of the scaffolds are complex and include chemical and biological composition, spatial architecture, mechanical and surface properties, and degradation kinetics. Polymeric scaffolds must provide adequate mechanical properties to match that of the host tissue and to aid the differentiation of certain cells. Architectural features have also an important role to mimic the functions of the native ECM. Thus, scaffolds must allow cell attachment and subsequent migration within the matrix, mass transfer of metabolites and enough space for the development of a system of vascularization and remodeling of the scaffolds of organized tissue.

Processing of polymeric nanofibers through electrospinning has gained much attention in the last decade due to its versatility for producing a wide variety of polymeric fibers as well as due to its ability to produce fibers in the submicron range that is otherwise difficult to achieve by using conventional fiber-spinning technologies (Bhardwaj and Kundu, 2010). Depending of a number of the intrinsic properties of the solution and processing parameters, uniform bead-free micro/nanofibers are collected in a grounded target, leading to the formation of a non-woven mat.

Therefore, characterization and quantification of the internal porous microstructure of polymeric scaffolds, surface area-to-volume ratio, spatial distribution, degree of interconnectivity, and orientation of the nanofibers are of great importance to the interpretation of the biological response of in vitro and in vivo tissue growth.

Conventionally, shape analysis is performed on binary images of the scaffold. Several indicators are used to measure the object area, perimeter, radius (of a circle with similar area), roundness factor, entropy, curvature and skeleton. However, the variability of the characteristics of gray level biomedical images often prevents obtaining binary images representing the objects of interest (Glasbey and Horgan, 1994; González and Woods, 1996; Castleman, 1979). Unlike standard techniques, morphological techniques are based on concepts of geometry, algebra, topology and set theory, to characterize structural properties of images (Facon, 1996; Serra, 1982, 1988 and 1992; Dougherty and Astola, 1994; Marshall and Sicuranza, 2006). The central idea of these techniques is to examine the geometric structures in an image by overlapping it with small size patterns, whose shape depends on the form of the components to be analyzed in the images, and the information that is to be obtained from the images. In this context, Mathematical Morphology provides a satisfactory solution for the analysis of shapes. Of all the techniques of analysis that belong to the field of mathematical morphology, the most appropriate tool, to characterize the shapes and their statistics, for both binary and gray level images, is the granulometric function, also called granulometric size distribution (Ballarin and Valentinuzzi, 2001; Heijmans, 1991; Vincent and Dougherty, 1994).

The aim of this work is to develop algorithms to compute adequate indices for characterization and quantification of shape, angle and size of biological components, as well as the statistical distribution of these characteristics. These features are extremely variable in the images of material with different manufacturing condi-

tions and different types of materials (Capes *et al.*, 2005; Lin *et al.*, 2003; Moore *et al.*, 2004).

This paper proposes the use of the granulometric size distribution on gray level images, using structuring elements of different shapes, and subsequent analysis of their moments in order to obtain features that characterize the images according to the number, shape and orientation of the components of the images. This technique was already applied to other research fields, obtaining very satisfactory results (Gonzalez *et al.*, 2009.a, b).

II. METHODS

A. Materials

For this study, 164 sample images belonging to 42 polymeric scaffolds of poly (L-lactic acid, NatureWorks PLA2002D) and poly(ε-caprolactone, Aldrich) obtained by electrospinning technique were processed. Electrospinning is an attractive technique for the preparation of polymeric scaffolds with specific morphologies, and it provides an opportunity to manipulate and control the surface area, fiber diameter, porosity and pore size, of the scaffolds. Figure 1 shows electrospun polymeric PLLA scaffolds. Different morphologies were obtained by varying the electrospinning setup (plate and tip collector), the intrinsic properties of the polymer solution (solvent mixtures and concentration) and processing parameters (applied voltage, distance needle-collector plate, distance needle–tip collector and speed of solution flow).

The microstructure of the obtained scaffolds was observed by scanning electron microscopy (SEM) (JEOL Model JSM-6460LV).

Of the 164 acquired images, 25 images belong to samples whose manufacturing process yielded nanofibers oriented in space. The images were acquired with a magnification of 1000X and 3000X.

The algorithms were developed in Matlab R14 using standard libraries for digital image processing with mathematical morphology.

B. Mathematical Morphology applied to binary images

This section describes the different operators used to process the images. As mentioned in the introduction, we used mathematical morphology because of its overall satisfactory results in the shape analysis. The basic operations of binary mathematical morphology are erosion and dilation. These operations compare subsets of the binary image with a pattern called a structuring element, which is translated across the entire image (Facon, 1996; Serra, 1982, 1988 and 1992).

Formally, the erosion of a set A by a structuring element E is defined as:

$$A\Theta E(x) = \{x \in A : E_x \subset A\} \qquad (1)$$

where E_x is the traslation of the set E by the vector x. The result of erosion is a binary image where the pixels are white when the structuring element is included within the subset of the analyzed image and is black otherwise.

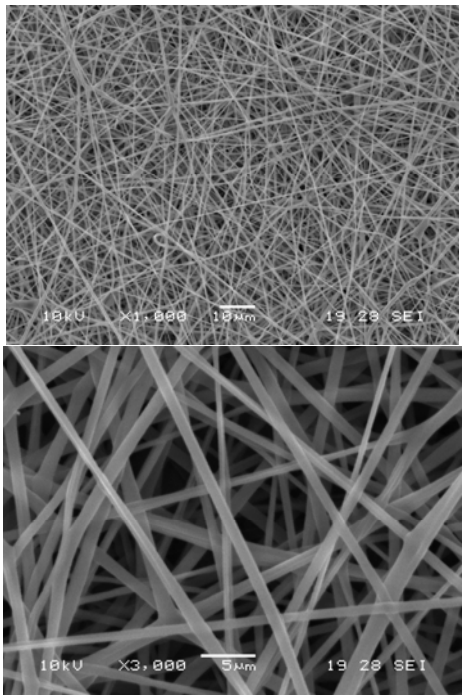

Fig. 1: SEM micrographs of polymer scaffolds obtained with the technique of electrospinning (Magnification: 1000X and 3000X).

Similarly, the dilation of A by the structuring element E is defined as:

$$A \oplus E(x) = \{x \in A : E_x \cap A \neq \varnothing\} \qquad (2)$$

In the dilation is assigned a white pixel if at least one pixel of intersection between the subset of the original image and the shifted structuring element and a black pixel when the intersection is empty. Dilation is a growing operation while erosion is a contraction operation.

From these basic operations new morphological operators are defined. For example, the opening is defined as erosion followed by dilation, that is:

$$A \circ E(x) = (A\Theta E) \oplus E \qquad (3)$$

The closing is defined as dilation followed by erosion, that is:

$$A \bullet E(x) = (A \oplus E)\Theta E \qquad (4)$$

Morphological Granulometry, which is defined by the iterative application of openings, is a mathematical morphology tool that provides characterization of shapes and sizes of the objects present in an image. Given a family of images arising from the implementation of successive openings with structuring elements of increasing size λ, the Granulometric Size Distribution function is defined by:

$$G(\lambda) = 1 - \frac{\Omega(A \circ E_\lambda)}{\Omega(A)} \qquad (5)$$

where Ω is a measure of the resulting image. In the case of binary images Ω(A) is the area of the white part of the image.

C. Mathematical Morphology applied to gray level images

As in mathematical morphology for binary images, the basic morphological operations for images are gray level erosion and dilation. Given two gray level images f,

g, the erosion of the image f by the structuring element g is defined by:

$$f \Theta g(s,t) = \min_{\substack{(x,y)\in Dg \\ (s+x,t+y)\in Df}} \{f(s+x,t+y) - g(x,y)\} \quad (6)$$

For each pixel of the image, the erosion operation is defined as the minimum difference between the intensities of the shifted structuring element and the corresponding intensities of the original image.

Similarly, the dilation of the image f by the structuring element g is defined by

$$f \oplus g(s,t) = \max_{\substack{(x,y)\in Dg \\ (s-x,t-y)\in Df}} \{f(s-x,t-y) + g(x,y)\} \quad (7)$$

The opening of each pixel of the image is defined as the maximum value of the sum between the intensities of the subset of the original image and the corresponding intensities of the structuring element.

The opening operator and the granulometry density for gray level images are defined similarly to the binary operators, requiring additional normalization to comply with the properties of density functions.

To compute the granulometry, successive openings are applied to the original image, with structuring elements of increasing size. After that a measure is computed for each resulting image, being that measure the volume of the image for grey level images. These values are normalized to the volume of original image. The following equation describes this feature

$$G(\lambda) = 1 - \frac{\Omega(A \circ E_\lambda)}{\Omega(A)} \quad (8)$$

After obtaining the size distribution function, which is actually a probability distribution function, we compute its mean, standard deviation and energy. These values were used as statistics of the images.

In order to obtain a density function which is invariant to the brightness of the image, we used a Standard Granulometric Function (SGF) (see Eq. 9). This function normalizes the particle size using the volume obtained after applying the largest structuring element (EE). Derivation of this function yields a probability density function, which maximum value indicates the most common size for the structuring element. In these images, this information (the maximum of the density function) may not provide the complete statistics to characterize its orientation, due to the large number of irrelevant components that usually exist in the image. For this reason it is necessary to analyze the statistics of the full function to have more accurate data for subsequent quantification

$$G(\lambda) = 1 - \frac{\Omega(A \circ E_\lambda) - \Omega(A \circ E_N)}{\Omega(A) - \Omega(A \circ E_N)} \quad (9)$$

D. Different stages of the proposed algorithm

To process the images, first we filtered the images, then we computed the gray-level Standard Granulometric Function and finally we obtained the first three moments of this function.

• Step 1: We applied a median filter with a 3x3 window to the test images, to remove the noise present in them.

• Step 2: We determined the gray-level Standard Granulometric Function (SGF) from the whole gray level images. In this way we obtained a probability distribution function normalized and invariant to possible changes in the brightness (light) images. This function was computed for different structural elements, depending on the objects of interest. The structuring elements applied were square, circular and linear with slopes from 0 ° to 180º, with steps of 10º. These elements were chosen because they correspond to the shapes of the nanofibers. This SGF for a sample image is shown in Fig. 2.

• Step 3: We obtained the first three moments of the SGF (mean, standard deviation and entropy). These moments are used as characteristics of the shapes on the image. Table 1 shows an example of specific times to an image.

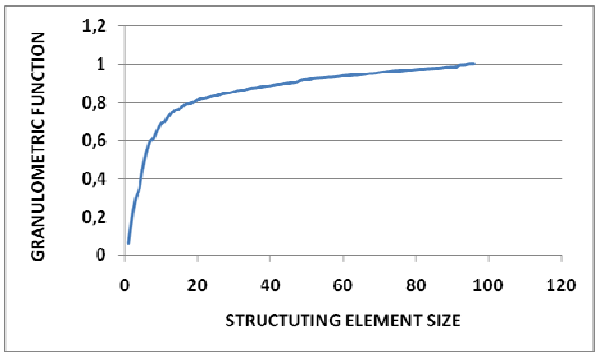

Fig. 2: Standard Granulometric Function (SGF)

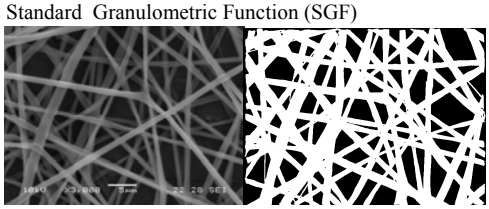

a) b)

Fig. 3: a) Original image, b) image where the nanofibers were defined by the expert and subsequently be binarized.

Table 1: Moments obtained from SGF with circular, square and linear the structuring elements.

Picture Name	Element	Angle	Mean Value	Standard Deviation	Entropy
S11-1000x.tif	Circular	0	0.839762	0.266602	-0.036286
S11-1000x.tif	Square	0	0.738165	0.308384	-0.033852
S11-1000x.tif	Linear	0	0.622669	0.302379	-0.017636
S11-1000x.tif	Linear	10	0.612285	0.305525	-0.017278
S11-1000x.tif	Linear	20	0.613333	0.303205	-0.016410
S11-1000x.tif	Linear	30	0.618862	0.300876	-0.017897
S11-1000x.tif	Linear	40	0.619443	0.302314	-0.017502
S11-1000x.tif	Linear	50	0.607675	0.302543	-0.015657
S11-1000x.tif	Linear	60	0.606470	0.300709	-0.015516
S11-1000x.tif	Linear	70	0.604909	0.300449	-0.015342
S11-1000x.tif	Linear	80	0.595066	0.302813	-0.014374
S11-1000x.tif	Linear	90	0.603328	0.301523	-0.014900
S11-1000x.tif	Linear	100	0.593958	0.305364	-0.014080
S11-1000x.tif	Linear	110	0.595137	0.302367	-0.013651
S11-1000x.tif	Linear	120	0.596378	0.299393	-0.014425
S11-1000x.tif	Linear	130	0.611051	0.303000	-0.015773
S11-1000x.tif	Linear	140	0.600481	0.298633	-0.014194
S11-1000x.tif	Linear	150	0.610388	0.301736	-0.016078
S11-1000x.tif	Linear	160	0.617440	0.300684	-0.017076
S11-1000x.tif	Linear	170	0.608565	0.300989	-0.016416

• Step 4: Finally, we analyzed the differences of these moments for the different morphological characteristics of the images. The characteristics evaluated in this study were the degree of occupation, the slope, the spatial distribution and thickness of the polymer.

III. RESULTS

In order to evaluate the morphological characterization of the fibers by the granulometric moments, we compared these moments to shape parameters computed manually on the images (reference parameters). Morphological characteristics were determined by an expert, who highlighted the lines that corresponds to the fibers and delimited manually the nanofibers present in the images (see Fig. 3). Subsequently the moments from the SGF, using structuring elements of different shapes were compared to the reference parameters, provided by the expert, to confirm the relations between the morphological characteristics and the computed moments.

A- Variations of the SGF moments for each type of sample.

In a first stage we determined the variation of the values of the moments of the SGF computed over each sample. As mentioned in the introduction, each sample has nanofibers with different morphologies, depending on the type of polymer and manufacturing parameters. Figure 4 shows the maximum variation of the moments of the images for each sample. It can be seen that, of 42 samples, only six of them showed variations in the moments greater than 0.04. This result indicates that the images acquired in each sample have moments that vary minimally between them and therefore can be used to characterize them.

B- Choice of image resolution.

The SGF and their respective moments were computed on images acquired with 3000X and 1000X magnification. The images acquired with a magnification of 1000X were used to properly characterize the morphology of the scaffolds; however, analysis of diameters was not carried out properly in these images due to the large number of very small diameter nanofibers, where the computed moments did not show a direct relationship with this parameter.

On the other hand, images acquired with a magnification of 3000X times characterized several parameters and then faithfully contributed to the characterization of the morphology of the scaffolds.

C. Definition of the parameters of the SGF.

One of the parameters necessary to compute the SGF is the maximum size of structuring element used for the morphological openings. The election of this parameter must take into account both the computational cost of the algorithm that uses it, and that the moments of the SGF must be a good characterization of the morphology of the images. To choose a value, we determined the SGF for a final size, N, using different values. First we used fixed values for N and second we used a variable value N as a function of the dimensions of the image. A fixed N did not allow to successfully compare the different morphologies of the images, possibly because of

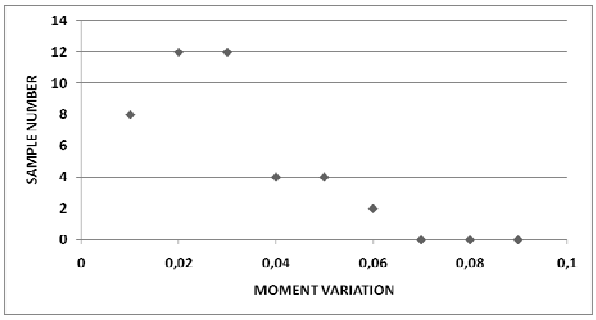

Fig. 4: Maximum variation of the moments of SGF determined for the images belonging to each of the 42 samples.

the variations in the size of the images. On the other hand, when using values N dependent on the image size, but of magnitude smaller than the sizes of the nanofibers, the results did not reflect the different morphologies. From all other values for N, as function of the image size, but of larger size, which gave a correct characterization of the morphology, the smaller value was chosen, in order to reduce the computational cost. The value chosen for N was one eighth of the height of the image, (size/8).

Also, in the computation of the SGF we have to define a method to prevent the edge of the images SGF leading to erroneous or unrepresentative results. This is because the morphological operators cannot be defined precisely in the pixels of the edge of the image, since the structural element in these pixels lies partially outside the domain of the image. It is therefore necessary to define what to do in this situation. One technique to avoid this issue is based on extending the original image so that when the structuring element is positioned at the edges, morphological operators can be determined correctly. The extension can be obtained either by reflection or by tiling the image in the borders. Since the nanofibers are oriented, this results in non-existent new orientations, and the orientation is a feature to quantify, so this technique cannot be used. Also it is possible to use a fixed gray level on pixels beyond the edges, of 255 when the image is eroded and of 0 when it is dilated. This method has the advantage that the value of edge pixels added to the image does not influence the computation of the openings. The latter technique was chosen with very good results.

On the other hand, all the moments obtained using the square element did not produce good morphological characteristics. Neither the standard deviation and energy showed significant variations in the test images examined, so these moments were not used in the analysis of this work for such images.

D- Change in occupancy with SGF moments.

The magnitude of the maximum average value obtained from the SGF, determined with linear structuring elements, is related analytically to the presence of objects of interest, which in this case are linear polymeric nanofibers, ie, related to the degree of occupation of the image.

Figure 5 shows the SGF determined for two images, one with a greater number of nanofibers than the other.

In the case where there are a greater number of fibers the average value of the SGF is larger. This result was observed in all images analyzed (see Fig. 6).

To compare these features, a gold standard binary image was used. With the help of a skilled expert, the percentage of area occupied by nanofibers was determined. These values were normalized according to the dimensions of the image. On the other hand the SGF mean value was computed for each image using linear structuring elements in the 18 directions proposed.

Figure 6 shows the relationship between the average linear values, determined using the proposed algorithm, and the occupancy of the nanofibers present in each image, as defined previously with the assistance of the expert. As can be seen in this figure, the average value increases with the occupancy rate, and this relationship is approximately linear. The image analysis shows that this behavior of the SGF was consistent over all processed images. At a later stage, this information could be used to determine the occupation rate directly from the SGF moments. This figure shows that the proposed algorithm is able to differentiate occupancy rates that varies above 10%.

E. Mean Value variability for the orientations present in the images.

Linear structuring elements were applied using the 18 proposed orientations. Consequently, for each image there are 18 respective SGFs with their moments. The analysis showed that in all the samples, in which the nanofibers were observed in all directions, the average values of the SGF for each image, determined using structural elements in the 18 directions, did not vary in magnitude (see Fig. 7). By contrast, when the nanofibers showed some particular orientation, the average values of the SGF obtained for each image varied significantly.

Figure 8 shows both situations. This image shows the variation of the mean value is minimal for cases where nanofibers are placed in all directions. On the other hand, when there nanofibers located in only a few dominant orientations, the mean maximum corresponded to the prevailing orientations and produce more than a maximum mean value or local maximum. This behavior was observed for other test images.

Another important finding in this regard was that the orientation associated to the maximum mean values was consistent with the orientations dominant in the image.

To corroborate this result we determined the variation of mean (Maximum Mean Value minus Minimum Mean Value) of the SGFs based on linear structuring elements, obtained from images with both aligned nanofibers and nanofiber oriented in all directions. Figure 9 shows a histogram of the values obtained, where it can be seen that this value is always below 0.09 for images where the nanofibers do not have a particular orientation, and is above 0.09 for nanofibers with some orientation.

In summary, for the test images examined, we can say that the SGF can determine, to some extent, if the membranes have oriented nanofibers in some direction, and what is such orientation.

F. Variation of the moments of the SGF with the thickness of the polymer.

The diameter of the nanofibers and their variability were found to be related to the moments of the SGF determined using a round structuring element. The

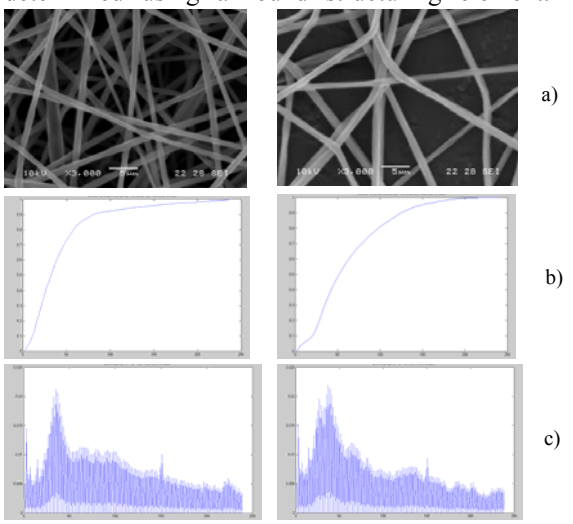

Fig. 5: a) SGF, b) the mean value and c) its derivative for two images of polymer scaffolds.

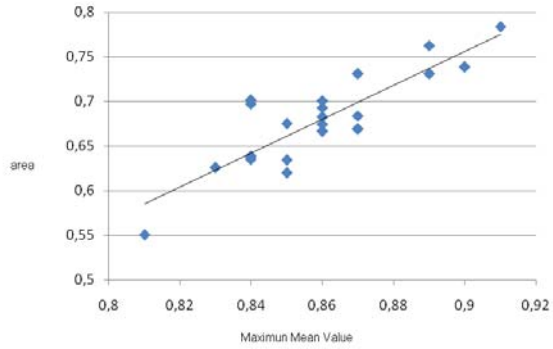

Fig. 6: Variation between the areas occupied by the nanofibers and the average value of the SGF.

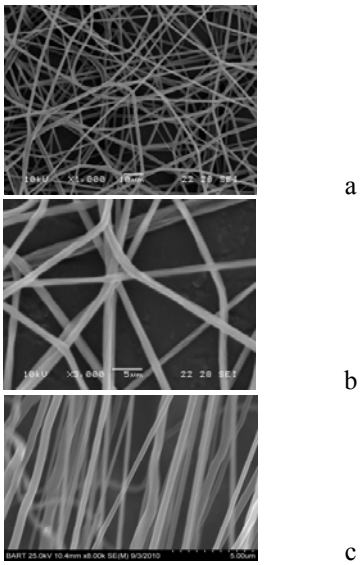

Fig. 7: SEM micrographs corresponding to the graph of a) and b) several nanofibers not preferentially oriented and c) several nanofibers oriented at 90 º.

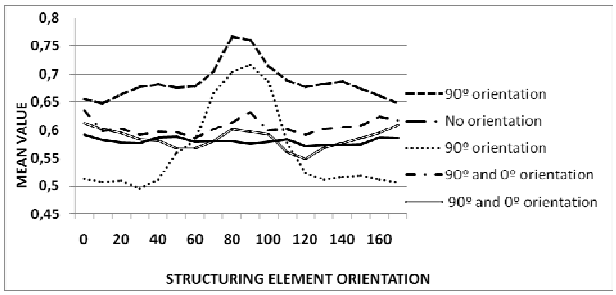

Fig. 8: Variation of the maximum value of the SGF for the different orientations of polymer nanofibers.

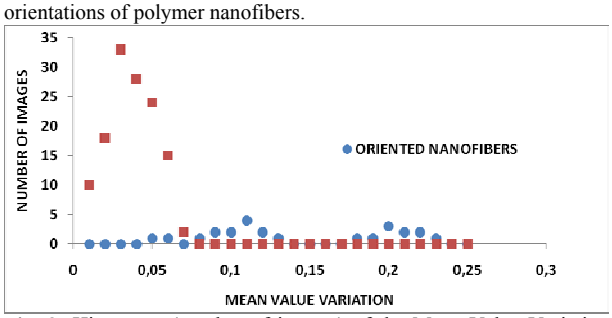

Fig. 9: Histogram (number of images) of the Mean Value Variation (Maximum Mean Value minus Minimum Mean Value) for aligned and unaligned nanofibers.

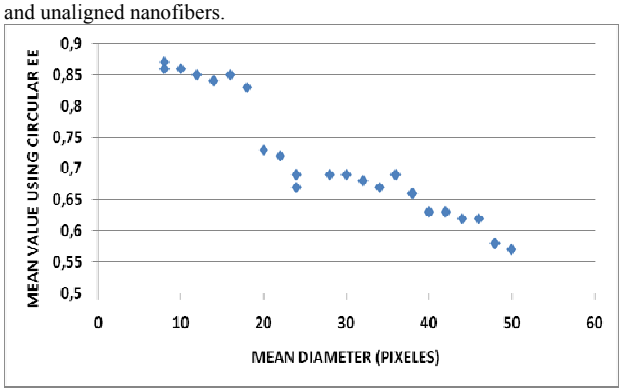

Fig. 10: Mean value determined SGF using a round structurtiring element vs. the average diameter of polymer nanofibers.

average values of SGFs with larger magnitude corresponded with smaller diameter of nanofibers and, in turn, larger diameter of nanofibers resulted in lower mean values. For each image the average diameter was measured with the help of the expert. This value is displayed in pixels, as each magnification of the sample corresponds to a different real diameter. Figure 10 shows this variation graphically. It is important to note that this method, used to determine the average diameter, is less sensitive than the expert measurement. This is due to the fact that different average diameters result in the same mean value for the SGF. However this value could be used as an index to sort the diameter of the nanofibers with diameters differing by more than 10 pixels, being of great help to the expert in the characterization of this parameter in the different images.

IV. CONCLUSIONS

After choosing the appropriate parameters, the moments obtained from the SGF are a good characterization of the morphology of the nanofibers present in the images under analysis. The occupancy rate, orientation and diameter of the nanofibers were fairly characterized by the proposed algorithm. One of the main advantages of this algorithm is that it is not necessary to binarize the images. In addition, the SGF has the advantage that it provides features not only on the morphology of the nanofibers, but also on its statistics.

From this work, taking into account the results obtained, we will work on developing software that can be used by the expert to quantify the morphological characteristics of such images. This software would be helpful to specialists in fibrous polymeric scaffolds, whom perform usually visual determination of these characteristics, and also allow them to evaluate the different morphologies with other measures of the shapes of the fibers.

REFERENCES

Abraham, G.A., P.C. Caracciolo, F. Buffa and T.R. Cuadrado, "Diseño y Preparación de Matrices Poliméricas Porosas para Ingeniería de Tejidos Biológicos," *Anales de la Academia Nacional de Ciencias Exactas, Físicas y Naturales*, **59**, 115-130 (2007).

Ballarin, V. and M. Valentinuzzi, "Segmentación en imágenes de Resonancia Magnética de Cerebro utilizando Morfología Matemática," *Actas del Congreso Argentino de Bioingeniería,* Tafí del Valle, Tucumán (2001).

Bhardwaj, N. and S.C. Kundu, "Electrospinning: A fascinating fiber fabrication technique," *Biotech. Adv.*,**28**, 325-347 (2010).

Castleman, K.R., *Digital Image Processing*, Prentice Hall (1979).

Capes J.S., H.Y. Ando and R.E. Cameron, "Fabrication of polymeric scaffolds with a controlled distribution of pores," *Journal of Materials Science: Materials in Medicine,* **16**, 1069-1075 (2005).

Dougherty, E.R. and J. Astola, *An introduction to nonlinear image prossesing,* Tutorial Texts in optical engineering, **TT16** (1994).

Facon, J., *Morfología Matemática. Teoría y ejemplos,* Curitiba Brasil, CITS (1996).

Glasbey, C.A. and G.W. Horgan, *Image analysis for the biological science,* Statistics in Practice, Series Editor Vic Barnett., Jonh Wiley and Sons (1994).

González, R. and R. Woods, *Tratamiento Digital de imágenes*, Addison Wesley (1996).

Gonzalez, M., V.L. Ballarin, A.R. Celín, V. Sánchez, M. Rapacioli and V. Flores, "Análisis de axones en crecimiento mediante la función Granulométrica de Tamaños," *XVII Congreso Argentino de Bioingeniería- VI Jornadas de Ingeniería Clínica (SABI),* Polo Tecnológico Rosario (2009a).

Gonzalez, M.A., J.I. Pastore and V.L. Ballarin, "Análisis de la morfología de los poros en muestras de materiales", *Reunión de Procesamiento de la In-*

formación y Control, Rosario (2009b).

Heijmans, H., "Theoretical aspects of gray-scale morphology," *IEEE Trans. Pattern Anal. Mach. Intell.*, **13**, 568-582 (1991).

Ikada, Y., "Challenges in tissue engineering." *J.R. Soc. Interface*, **3**, 589-601 (2006).

Lin, A.S., T.H. Barrows, S.H. Cartmell and R.E. Guldberg, "Micro-architectural and mechanical characterization of oriented porous polymer scaffolds," *Biomaterials*, **24**, 481-489 (2003).

Marshall, S. and G. Sicuranza, *Advances in nonlinear signal and image processing*, Eurasip (2006).

Moore, M.J., E. Jabbari, E.L. Ritman, L. Lichum, B.L. Currier, A.J. Windebank and M.J. Yaszemski, "Quantitative analysis of interconnectivity of porous biodegradable scaffolds with micro-computed tomography," *Journal of Biomedical Materials Research* Part A, **71A,** 258-267 (2004).

Serra, J. , *Image Analysis and Mathematical Morphology*, Academic Press, London (1982).

Serra, J., *Image Analysis and Mathematical Morphology*- Part II: Theoretical Advances,, Academic Press, London (1988).

Serra, J. *Image analysis and Mathematical Morphology,* Academic Press (1992).

Vincent, L. and E. Dougherty, *Morfological Segmentation for Textures and Particles,* Digital Image Processing Methods, Rochester, New York (1994).

Received: March 1, 2011.
Accepted: May 9, 2011.
Recommended by Subject Editor Ricardo Gómez.